Electronic Supplementary Material (ESI) for Sustainable Energy & Fuels.

Supplementary Information

FTIR-Operando study of the photocatalytic reduction of CO_2 in presence of water vapor over Pt/TiO_2: on the role of surface residual C-species

Joudy Dankar,* Céline Pagis, Mickael Rivallan, Mohamad El-Roz*

Materials and Methods

- **TiO_2-UV100**

Commercial TiO_2 powder of Hombikat UV100 was obtained from Sachtleben Chemie GmbH. Various analyses have been carried out on this material (Figure S1). XRD confirms that it consists of 100% anatase crystalline phase with an average crystallite size of 8 ± 0.8 nm (Scherrer method). Its BET surface is 316 ± 16 m²/g, and it possesses an indirect band gap energy of 3.31 eV (determined by UV-Visible spectroscopy). Elemental analysis by XRF reveals some impurities in the TiO_2-UV100 in the following quantities: P 0.18 wt%, S 0.08 wt%, Nb 0.02 wt%, Zr 0.02 wt%. Commercial TiO_2 is selected as a model photocatalytic system of choice in order to minimize experimental variability and to obtain reproducible and comparable results with literature.

- **Pt/TiO_2-UV100**

Deposition of platinum was carried out via an impregnation reduction method, which allows optimized deposition yields of metallic nanoparticles [1]. This method consists of a step of impregnation of the metal precursor followed by chemical reduction without a protective agent.

Typically, 1 g of TiO_2-UV100 is introduced into 100 mL of H_2O, to which 400 µL of an aqueous solution of H_2PtCl_6 at 0.256 M are added. The mixture is stirred for 45 minutes, then 5.08 mL of an aqueous solution of sodium borohydride $NaBH_4$ at 0.1 M (Pt/$NaBH_4$=1:5 mol.mol-1) is added and stirred for 15 minutes. The mixture is then filtered and washed with 1 L of permuted H_2O, and the recovered gray solid is dried under air at 100°C for 24 h.

The obtained Pt/TiO_2 catalyst contains 1.78 wt% Pt (determined by ICP-AES), a BET surface area of 300 ± 10 m²/g (Figure S1), and an average crystallite size of 9 ± 0.8 nm (Scherrer method).

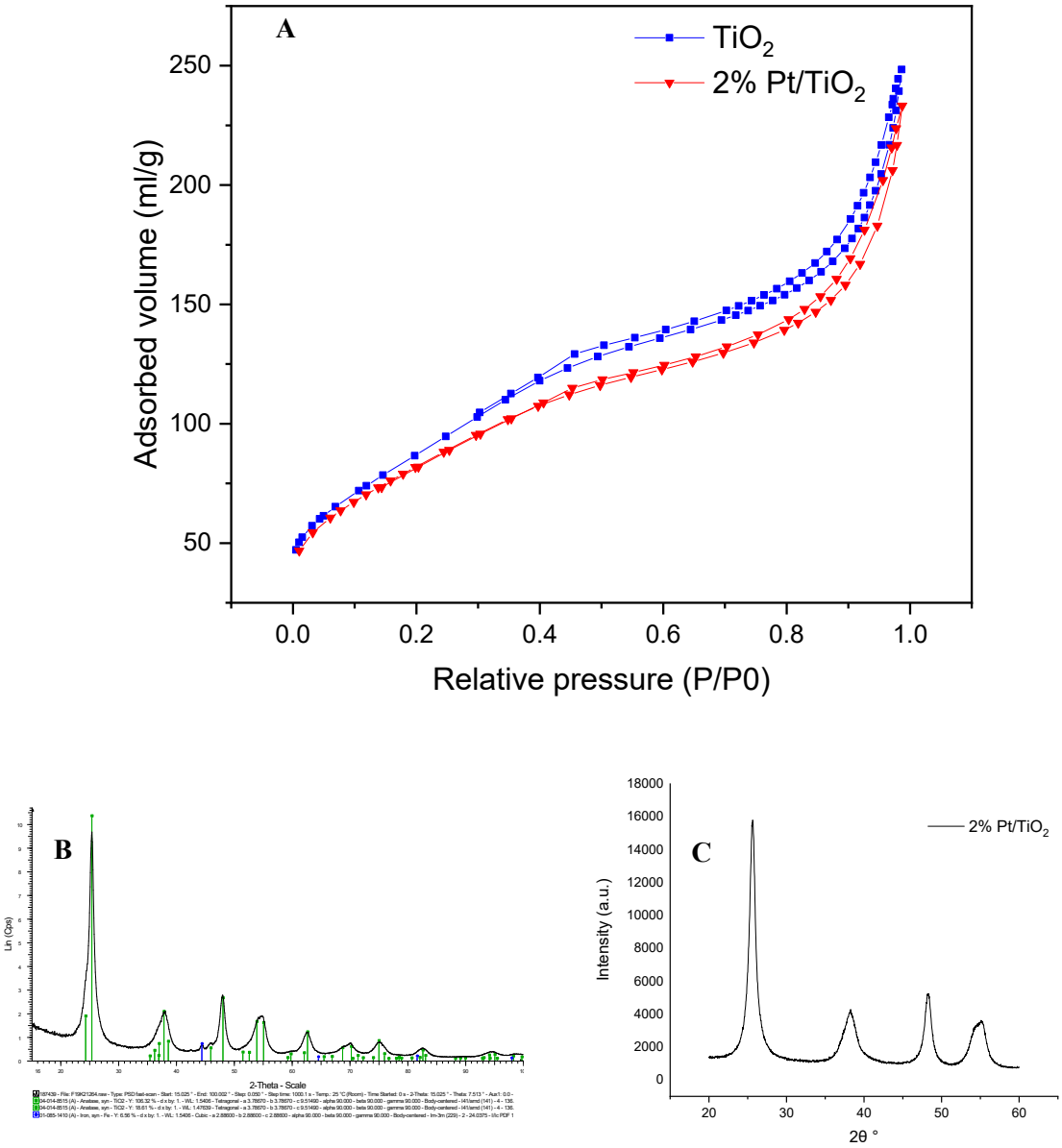

Figure S1. Characterization of TiO_2 and Pt/TiO_2 catalyst: (A) N_2 physisorption isotherms after degasification at 350°C and XRD patterns for (B) TiO_2 and (C) Pt/TiO_2, revealing pure crystalline anatase phase and small particle size.

IR *Operando* photoreactor

The photocatalytic reduction of carbon dioxide was performed using an *operando* IR photoreactor developed at *Laboratoire Catalyse et Spectrochimie (LCS)*, illustrated in Figure S2. This photoreactor has already been used to elucidate photocatalytic reaction mechanisms under real conditions, in particular the photooxidation mechanisms of methanol on the surface of TiO_2-P25 (Evonik-Degussa) [2]. Photocatalysts are pressed into self-supported pellets (Ø =16 mm, m ≈ 10 ± 1 mg/cm^2) and placed in the center of the photoreactor. FTIR spectra of the outlet gas phase and of the surface are collected with a Nicolet 5700 FTIR spectrometer (64 scans/spectrum) equipped with an MCT detector. At the outlet of the reactor, the gaseous composition is analyzed by mass spectrometry, while complementary information on the gas phase can be simultaneously gained by means of IR spectroscopy with a gas micro-cell.

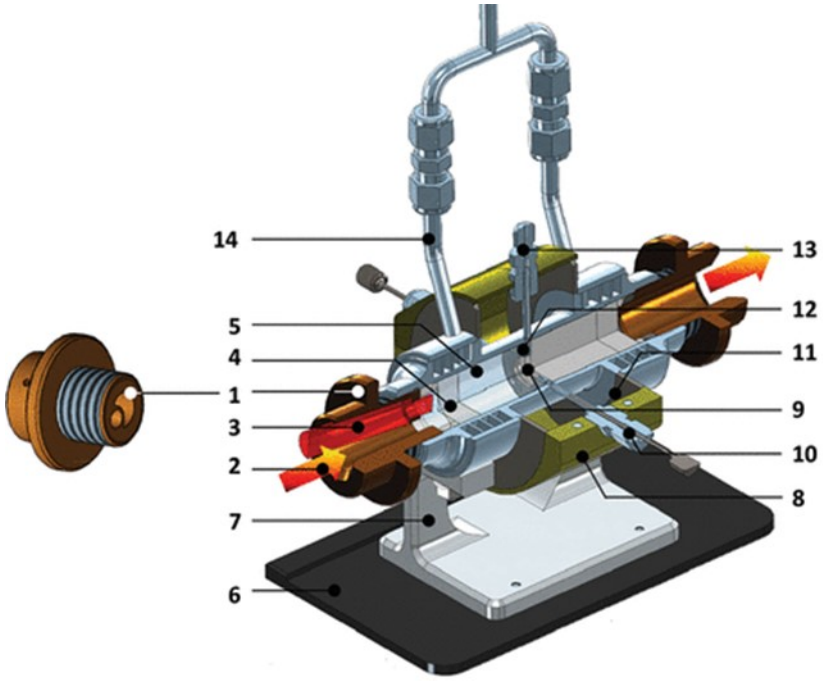

Figure S2. Scheme of operando photoreactor IR transmission setup developed at LCS: (1) Adjusting nut for airtightness (modified for UV-Vis guide position), (2) IR beam, (3) UV-Vis light guide, (4) Kalrez O-ring, (5) KBr window, (6) spectrometer base plate, (7) IR cell support, (8) oven location, (9) sample wafer, (10) gas inlet, (11) external shell, (12) wafer holder, (13) thermocouple location, (14) air cooling outlet, (15) gas outlet, (16) air cooling inlet.

The exact reaction conditions adapted for our test under CO_2 photocatalytic reduction are summarized in Table S1. The irradiation spectra of lamp used in this study is displayed in Figure S3.

Table S1. List of operating conditions used for CO_2 reduction photocatalytic tests.

Flow rate (CO_2 or Ar)	5 cc/min
H_2O	20 000 ppm (RT)
Lamp power	150 W/m² [@365nm]
Type of lamp	Hamamatsu Xe Lamp
Irradiated surface area	~ 2 cm²
Catalyst amount	~ 20 mg
Bed temperature	20 °C
Catalysts	Pt(2%)/TiO_2-UV100 TiO_2-UV100
Dead volume of reactor	0.42 cm^3
Gas phase analysis	Mass spectrometry, IR

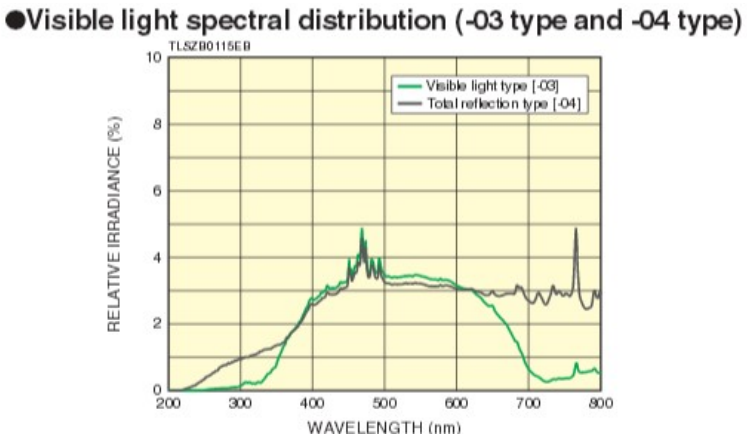

Figure S3. Irradiation spectra of the Xe (-03 type) lamp used in this study. The Xe lamp gives a continuous spectrum from UV to the visible spectral range.

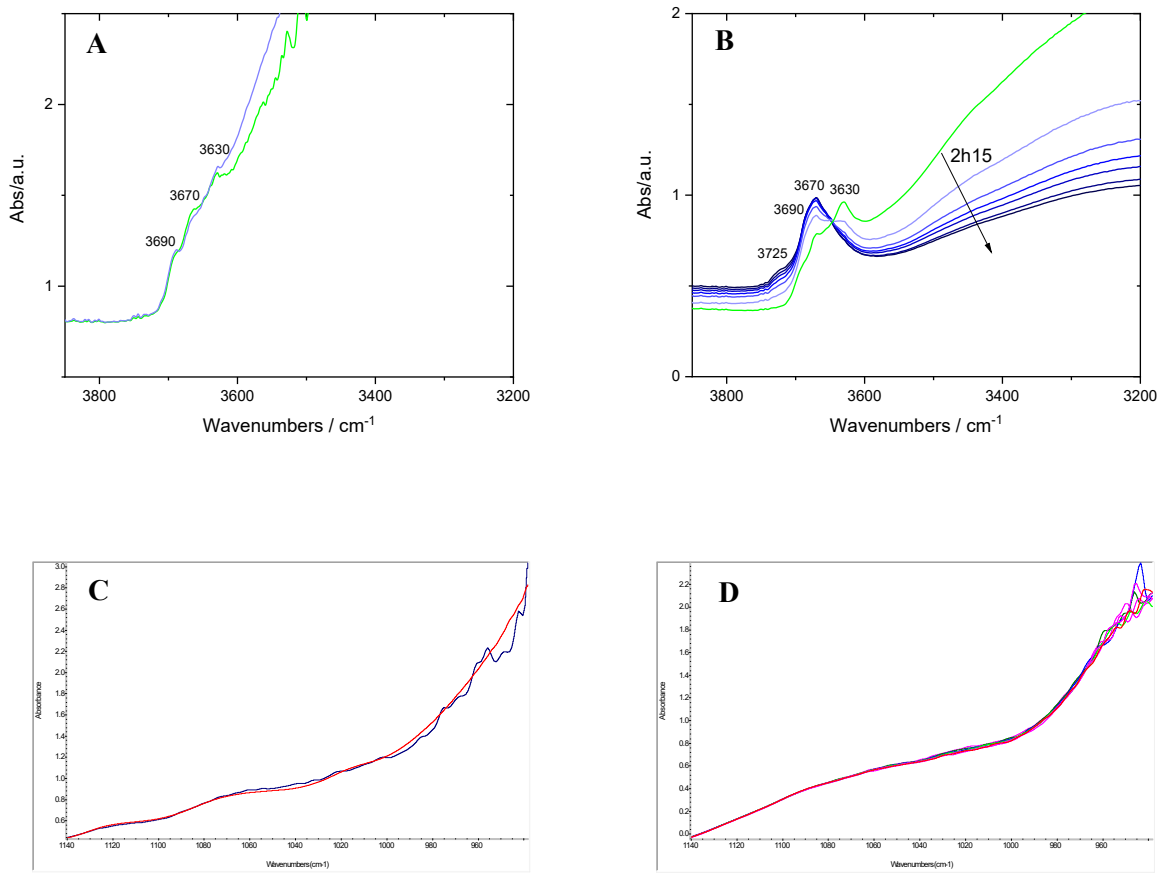

Figure S4. Evolution of the IR spectra in the hydroxyl region upon UV-Vis irradiation of (A) TiO_2 (for 25 min) and (B) Pt/TiO_2 (for 135 min) surfaces, previously activated under Ar gas. In green, IR spectrum of the surface before irradiation. In (C) and (D) respective 1140-940 cm^{-1} region for TiO_2 and Pt/TiO_2 under irradiation.

$\delta(TiOH)^3$ expected at 1037 cm^{-1} is not evidenced under our operating conditions (Figures S4-C and D).

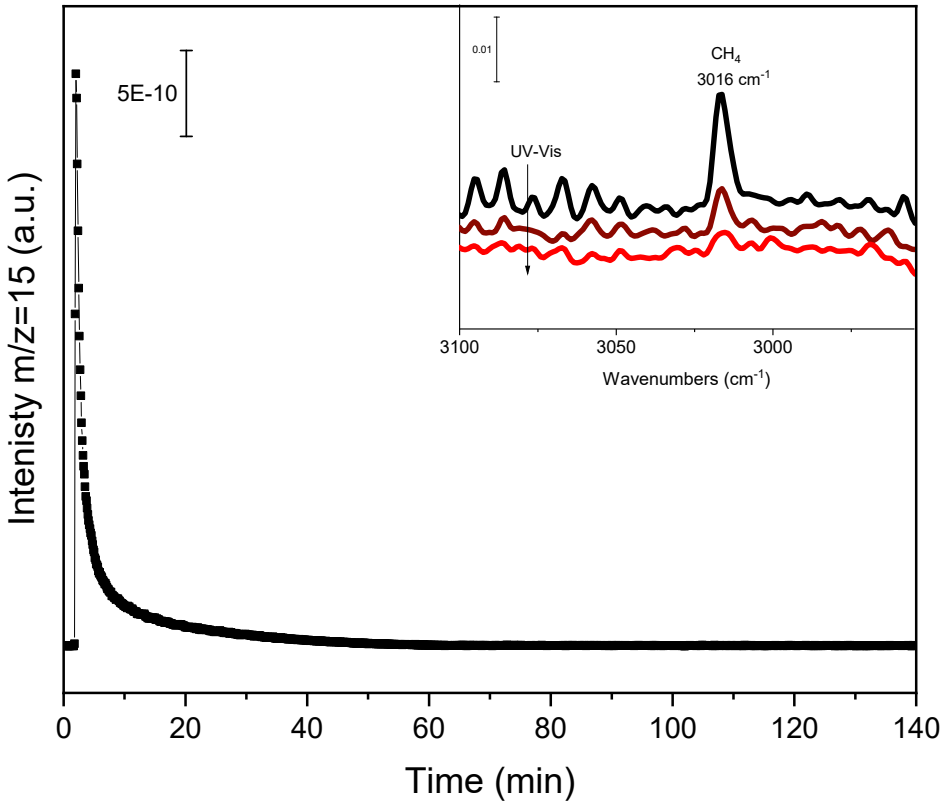

Figure S5. Evolution of mass spectra signal of CH_4 gas component (m/z=15) during 135 min UV-Vis irradiation under inert Argon gas on Pt/TiO_2 catalyst. The inset shows in situ FTIR gas phase spectra acquired during first five minutes of irradiation.

n.b. methane was monitored on the MS following mass number 15, due to contribution of H_2O on m/z=16.

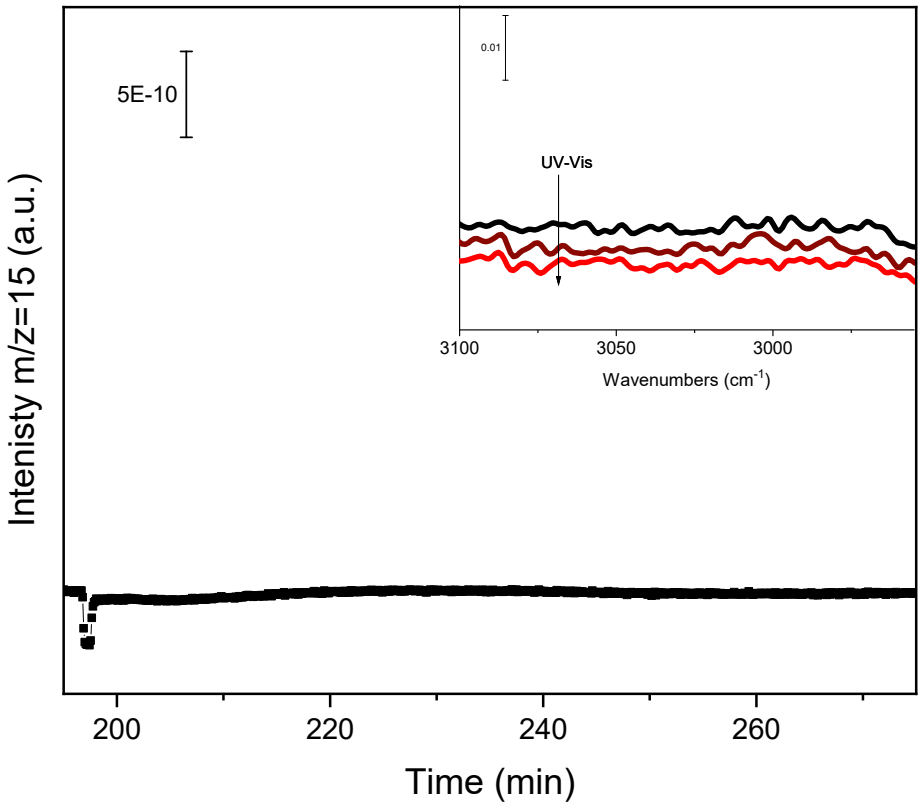

Figure S6. Evolution of mass spectra signal of CH_4 gas component during 80 min UV-Vis irradiation under CO_2/H_2O flow on Pt/TiO_2 catalyst. The inset shows in situ FTIR gas phase spectra acquired during first five minutes of irradiation.

n.b. methane was monitored on the MS following mass number 15, due to contribution of H_2O on m/z=16.

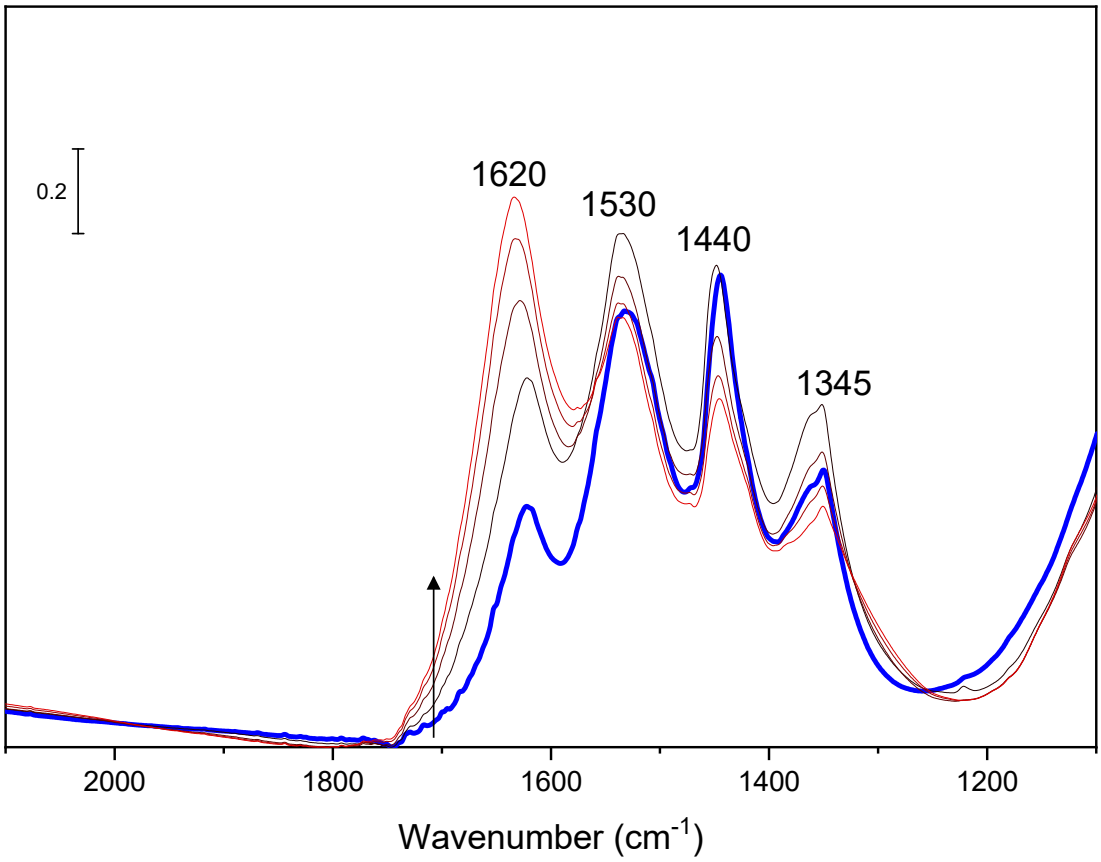

Figure S7. Evolution of the IR spectra of Pt/TiO_2 surface upon stopping UV-Vis irradiation while maintaining CO_2/H_2O flow for 25 min (from black to red spectrum). In blue, IR spectrum of the surface before stopping UV-Vis irradiation.

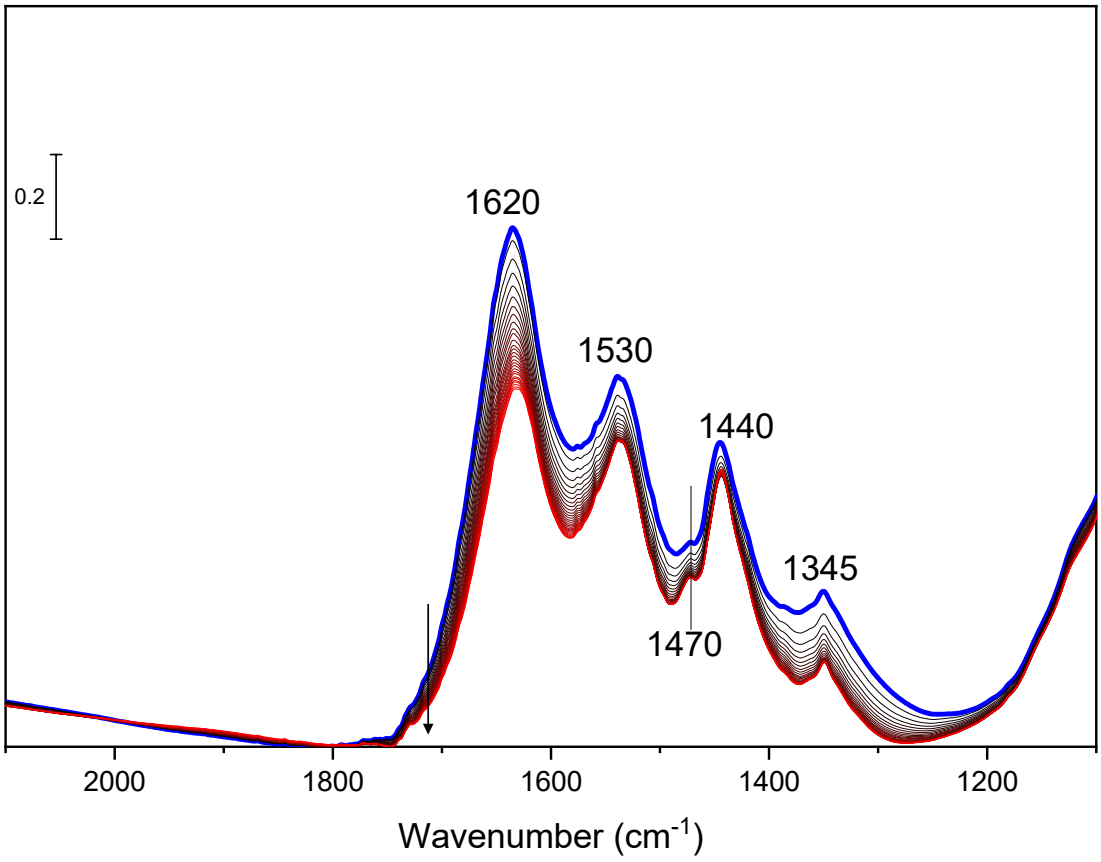

Figure S8. Evolution of the IR spectra of Pt/TiO_2 surface upon Ar flow for 60 min (from black to red spectrum). In blue, IR spectrum of the surface stabilized under CO_2/H_2O, before switching to Ar.

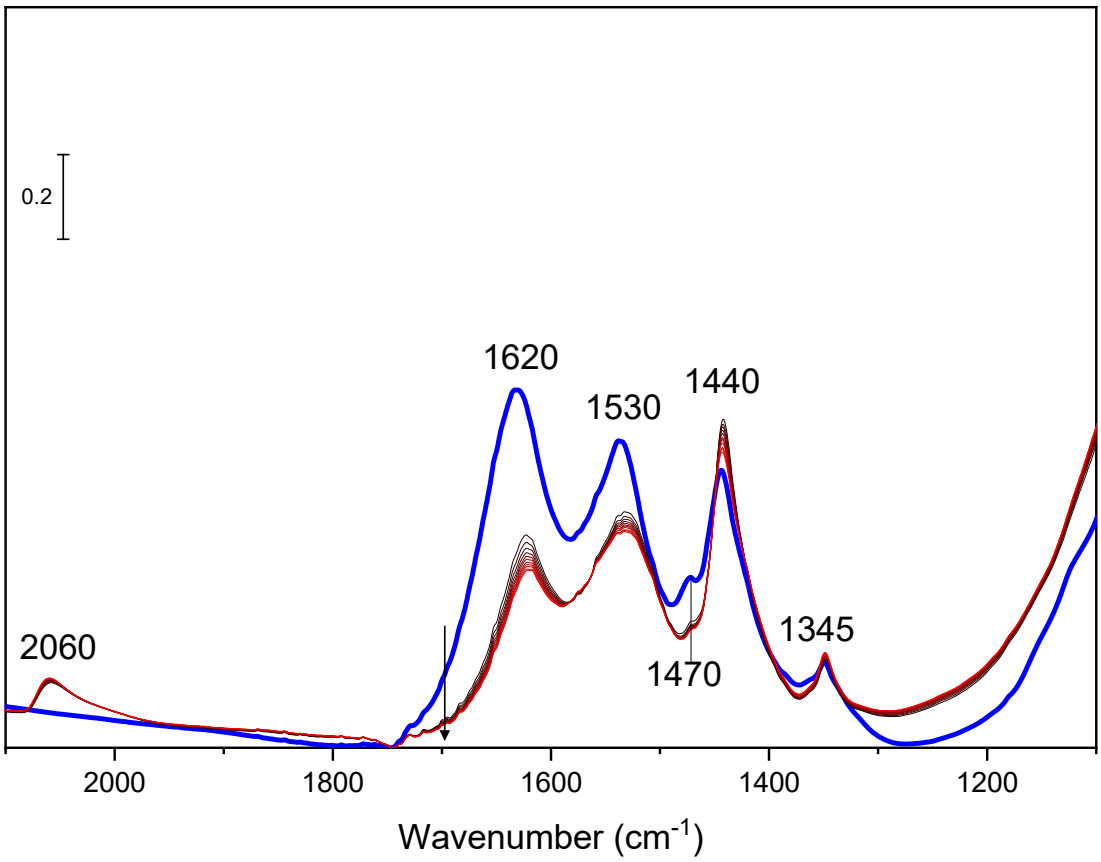

Figure S9. Evolution of the IR spectra upon UV-Vis irradiation for 25 min of Pt/TiO_2 surface previously stabilized under Ar gas (from black to red spectrum). In blue, IR spectrum of the surface before irradiation.

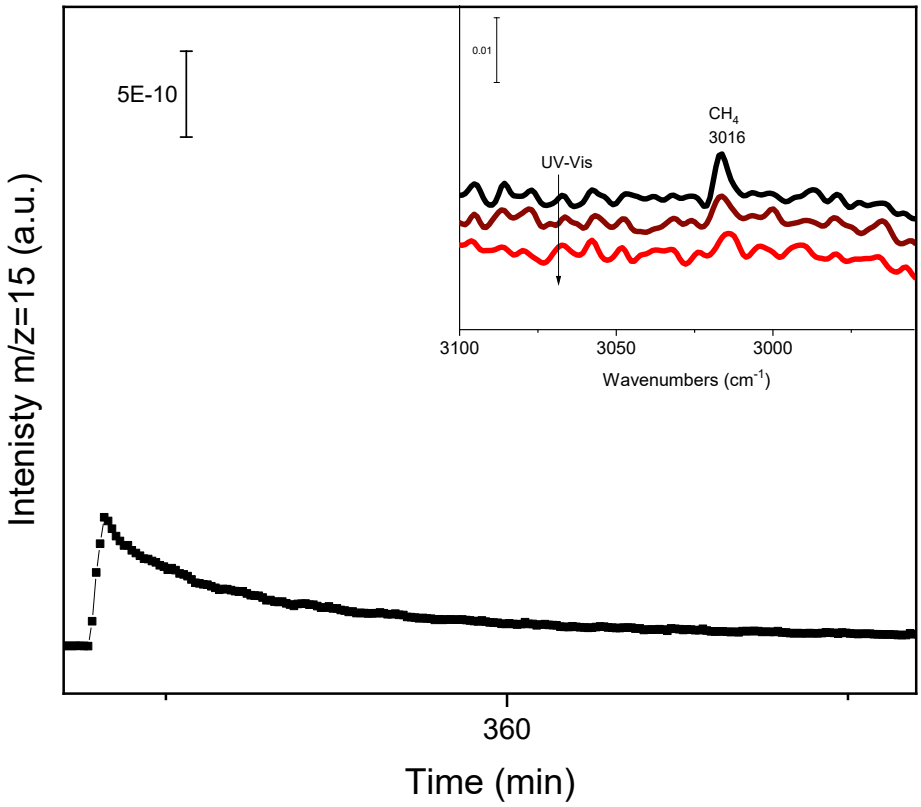

Figure S10. Evolution of mass spectra signal of CH_4 gas component during 25 min UV-Vis irradiation previously stabilized under Ar gas on Pt/TiO_2 catalyst. The inset shows in situ FTIR gas phase spectra acquired during first five minutes of irradiation.

n.b. methane was monitored on the MS following mass number 15, due to contribution of H_2O on m/z=16.

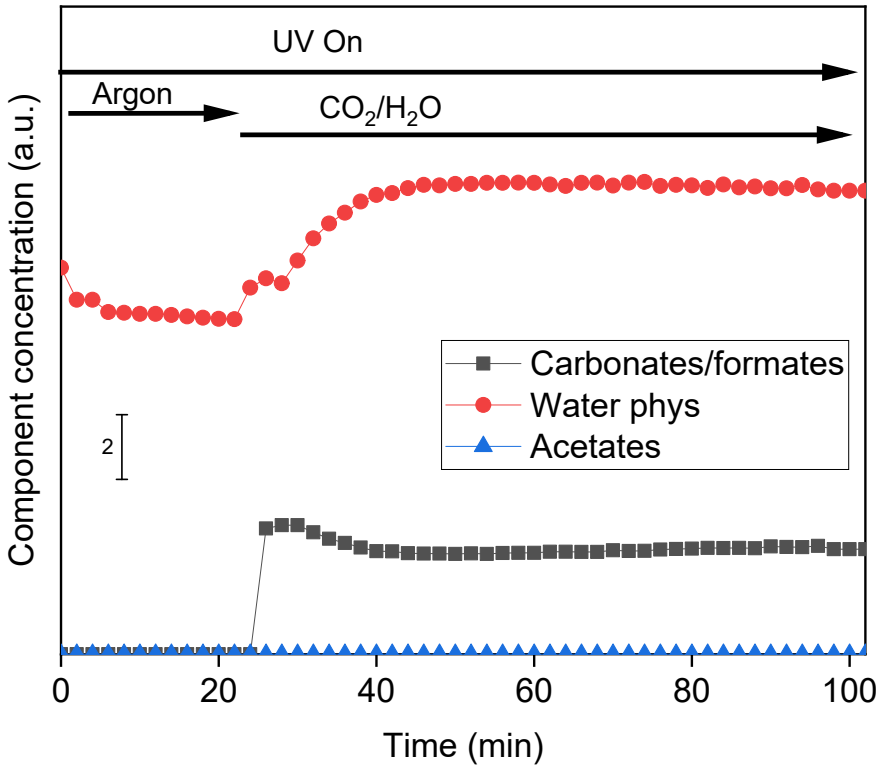

Figure S11: Component concentration profiles of carbonate and formate (grey), physisorbed water (red) and acetate (blue) obtained by MCR analysis of bare TiO_2.

Chemometric analysis shows that TiO_2 surface initially contains negligible amounts of C-species. Upon irradiation under inert Argon, a decrease in the quantity of physisorbed water is observed. Following 25 min of irradiation under inert flow, CO_2/H_2O reactant mixture is introduced. Under these conditions, chemometric evolution reveals an increase in surface water coverage, that is accompanied with an increase in carbonate/formate concentration. However, compared to Pt/TiO_2, formation of acetates is not observed on bare TiO_2.

Equations

$$\%Pt°CO = [Pt°CO]_{t=x}/[\ Pt°CO]_{max}*100 \qquad \text{Eq. (S1)}$$

$$\%CH_{4(g)} = [CH_{4(g)}]_{t=x}/[CH_{4(g)}]_{max}*100 \qquad \text{Eq. (S2)}$$

$$HCOO\ldots Ti + H_2O \rightarrow HCOOH_{(g)} + TiOH \qquad \text{Eq.(S3)}$$

$$CH_3COO\ldots Ti + H_2O \rightarrow CH_3COOH_{(g)} + TiOH \qquad \text{Eq.(S4)}$$

MCR-ALS: Attribution of principle component spectra (Figure 2)

Since spectral contributions observed in the 1800-1000 cm^{-1} region can be overlapping, a mathematical approach based on multivariate curve resolution (MCR) analysis using constrained Alternating Least Squares (ALS) algorithm was performed, using Unscrambler software. MCR-ALS is an algorithm that provides a bilinear decomposition of mixed experimental data into estimates of the corresponding profiles of the pure chemical species using a constrained Alternating Least Squares algorithm [4]. MCR-ALS applied to time-resolved spectroscopy data can generate resolved spectra of the individual component chemical species and their respective concentration profiles as a function of time. The MCR bilinear model is usually expressed as: D = CST+ E [5], where D is the raw data set consisting of multiple components (i.e., IR spectra recorded over time), S is the generated matrix of pure spectra, C is the respective concentration profiles for each of the pure components and E is the error matrix. ALS method is based upon minimizing E via an iterative least squares process.

The decomposed spectra (Figure 2) determined via MCR-ALS analysis are comprised of four individual components, revealing different spectral features that can be used to identify the nature of reaction intermediates. Component 1 consists of critical bands located at 1505 cm^{-1} and 1360 cm^{-1}, thus it is attributed to a mixture of formate and carbonate species. Component 2 possesses a main band contribution at 1635 cm^{-1} and is therefore the main contribution is assigned to physisorbed water. Meanwhile, Component 3 is signaled by fingerprint spectral modes at 1530 cm^{-1}, 1440 cm^{-1}, and can be attributed to the asymmetric and symmetric OCO stretching vibrations of adsorbed acetates. This assignment is supported by additional band at 1345 cm^{-1} that is attributed to the bending vibration δs(CH3) of the same species. Finally, Component 4 showcases a baseline spectrum that is characteristic of bulk TiO_2.

Table S2. MCR-ALS IR band assignment according to literature.

Assignment δ	Band frequency (cm^{-1})	Ref
Acetates		[6]
υas(COO)	1530	
υs(COO)	1440	
δs(CH3)	1345	
Formates/carbonates		[7]
υas(COO)	1505	
υs(COO)	1362	
Δ(HCO)	1378	

References

1 K. Guillois, L. Burel, A. Tuel and V. Caps, *Appl. Catal., A*, 2012, **415-416**, 1–9.

2 M. El-Roz, P. Bazin, M. Daturi and F. Thibault-Starzyk, *Phys. Chem. Chem. Phys.*, 2015, **17**, 11277–11283.

3 J. P. Smith, E. C. Holahan, F. C. Smith, V. Marrero and K. S. Booksh, *Anal.*, 2019, **144**, 5425–5438.

4 A. de Juan, J. Jaumot and R. Tauler, *Anal. Methods*, 2014, **6**, 4964–4976.

5 L.-F. Liao, C.-F. Lien and J.-L. Lin, *Phys. Chem. Chem. Phys.*, 2001, **3**, 3831–3837.

6 T. Yan, L. Wang, Y. Liang, M. Makaremi, T. E. Wood, Y. Dai, B. Huang, A. A. Jelle, Y. Dong and G. A. Ozin, *Nat. Commun.*, 2019, **10**, 2521.